α-Calcium sulphate hemihydrate with high aspect ratio crystalline as porous-structured biodegradable ceramic for bone regeneration

Anh Phuong Nguyen Hong[1], Dieu Linh Tran[1], Ngoc Thuy Trang Le[1], Quoc Vinh Ho[1], Minh Hoang Vo Do[1], Dang Khoa Vo Nguyen[1], Van Du Cao[2], Dai Hai Nguyen[1, 3*]

[1]Institute of Advanced Technology, Vietnam Academy of Science and Technology, 1B TL29 Street, Thanh Loc Ward, District 12, Ho Chi Minh City, Vietnam
[2]Lac Hong University, 10 Huynh Van Nghe Street, Buu Long Ward, Bien Hoa City, Dong Nai Province, Vietnam
[3]Graduate University of Science and Technology, Vietnam Academy of Science and Technology, 18 Hoang Quoc Viet Street, Nghia Do Ward, Cau Giay District, Hanoi, Vietnam

Received 27 April 2024; revised 27 May 2024; accepted 31 July 2024

Abstract:

Porous-structured bioceramics have emerged as an advanced approach in bone regeneration due to several advantages, including improved nutrient and oxygen diffusion, accessible space for cell attachment and proliferation, superior mechanical compatibility with surrounding tissues, and enhanced bone healing. Therefore, in this study, porous alpha-calcium sulphate hemihydrate (α-HH) was synthesised via a one-step salt solution method using calcium chloride. A key advantage of using calcium chloride in this method is that it not only improves the purity of the product but also promotes the formation of high-aspect-ratio α-HH crystals, thereby facilitating the development of a porous structure more effectively. The prepared porous α-HH was characterised using several modern analytical techniques, including Fourier transform infrared spectroscopy (FTIR), X-ray diffraction (XRD), thermogravimetric analysis (TGA), differential scanning calorimetry (DSC), and field emission scanning electron microscopy (FE-SEM). These analyses revealed that the synthesised powder met medical-grade standards and exhibited a porosity of 61.32%±3.2, with a compressive strength of 5.04±0.11 MPa. *In vitro* tests further demonstrated the material's commendable biodegradability, as well as its capacity for mineralisation, cell adhesion, and migration, suggesting that porous α-HH is a promising biomaterial for bone engineering.

Keywords: **biodegradable ceramic, bone regeneration, calcium sulphate hemihydrate, porous structure.**

Classification numbers: **2.2, 3.6**

1. Introduction

The reconstruction of large bone defects caused by biochemical disorders, tumour resection, or fractures presents a significant challenge for both orthopaedic and trauma surgery [1]. Traditional methods, such as autologous and allograft transplantation, face limitations, including high donor site morbidity and limited availability [2]. Consequently, there is growing interest in synthetic materials that may offer a reliable and effective alternative for bone regeneration. The need for advanced materials in bone regeneration has prompted extensive research into bioceramics, particularly those with improved porosity and mechanical properties. The porosity of biomaterials plays a crucial role in bone and tissue regeneration, as it provides space for cells to enter and grow while also allowing for the circulation of nutrients and oxygen, ensuring the survival and function of cells. This structure also facilitates the growth of new blood vessels, which is essential for bone regeneration [3, 4].

Regarding structural formation, porous bioceramics can be classified into two main types. The first type, characterised by a network of interconnected pores, voids, or spaces throughout the structure, is achieved using a range of methods such as foaming, cryogenic moulding, 3D printing, cavitation, partial sintering, and electrochemical methods [5, 6]. The second type is constructed from crystals with a high aspect ratio, where the elongated or needle-like crystals naturally create a porous structure. The high aspect ratio (where length is significantly greater than width) of these crystals prevents dense packing and enhances interlock, further contributing to the formation of a porous network and improving the mechanical properties of the materials. The main methods used to create porous materials in this second group involve chemical reactions to adjust crystal size and shape in the synthesis solution or phase transition processes to form amphiphilic structures with high-aspect-ratio crystalline phases [7-9]. Depending on the structural characteristics of the material and the specific application, the appropriate porous type is selected.

[*]Corresponding author: Email: nguyendaihai0511@gmail.com

Calcium sulphate hemihydrate (HH), a type of ceramic-based biomaterial, has already been utilised extensively in clinical applications for implanting non-load-bearing bone defects due to its excellent biocompatibility, osteoconduction, and osteointegration [10]. HH is biocompatible and biodegradable within several weeks of implantation, leaving behind a calcium-rich environment that promotes the proliferation of osteoblasts and facilitates bone regeneration. Moreover, compared to calcium phosphate bioceramics, HH exhibits a rapid self-setting ability within only 2-4 minutes [11, 12]. During the setting process, HH absorbs water, and a rearrangement of the water molecules occurs with the sulphate and calcium ions, forming the more stable dihydrate (DH) species and providing excellent mechanical properties for the material [13]. HH is typically synthesised from calcium sulphate dihydrate (DH) via a calcination process, which involves increasing the temperature to a certain level to reduce part of the water of crystallisation [14]. Recently, much research on α-HH has focused on synthesising it with various crystal morphologies through different methods to optimise the properties of α-HH for specific medical applications. By manipulating crystal morphology, scientists can control the mechanical properties, degradation rate, and porosity of α-HH, thereby creating materials capable of supporting bone regeneration more effectively [15, 16]. However, there are very few studies reporting on the development of porous α-HH based on its crystalline structure.

One notable study involved the preparation of α-HH nano-ellipsoids with a porous structure, as reported by G. Jiang, et al. (2015) [17]. The nano-ellipsoids of α-HH, measuring 600 nm in length and 300 nm in width, were prepared using a robust wet-chemistry method by mixing Ca^{2+} and SO_4^{2-} precursors in the presence of a mediating and capping agent, Na_2EDTA. The resulting porous nano-ellipsoids, with an average pore size of 38 nm, possessed a larger specific surface area (37.9 cm^3/g) than non-porous ones (3.8 cm^3/g). However, Na_2EDTA can form complexes with metal ions, particularly Ca^{2+}, resulting in the formation of EDTA-Ca complexes, which can lower the quality of the final product. In a previous study, we successfully synthesised rod-shaped α-HH using a salt solution method [18]. DH precursor was dehydrated into α-HH in a 5% $CaCl_2$ solution with H_2SO_4 and oleic acid. The presence of sulfuric acid enhances the dissolution of calcium sulphate dihydrate, increasing the concentration of Ca^{2+} ions in the solution, which facilitates the formation of calcium sulphate hemihydrate crystals. Meanwhile, oleic acid acts as a surfactant for monodisperse crystal preparation. Although the obtained α-HH demonstrated comparable regenerative efficiency to commercial bone grafts in *in vivo* experiments, the difficulty in removing these additives may increase the product's impurities, which could have undesirable effects in practical applications. Thus, more efficient methods are needed to create α-HH materials with controllable properties and higher purity.

Given the importance of porous structures and product purity, in this study, rod-shaped α-HH crystals with a high aspect ratio were prepared via a salt solution method from DH using only $CaCl_2$ at different concentrations as the salt medium. During the dehydration of DH in a Ca^{2+}-rich environment, crystal growth kinetics were induced on the surface of the (001) edge rather than the (100) edge, resulting in a stretching process that formed rod-shaped crystals [19]. Furthermore, the sole use of $CaCl_2$ salt solution as a crystal growth medium helps enhance the quality of the final product. The physicochemical properties of the synthesised α-HH, including structural quality and phase composition, were monitored through FTIR, XRD, and TGA/DSC. The size and rod-shaped crystal structure were evaluated via FE-SEM. Moreover, *in vitro* experiments were conducted to confirm the potential of these materials for further clinical applications.

2. Materials and methods

2.1. Materials

Calcium sulphate dihydrate (DH, 98%) and anhydrous calcium chloride ($CaCl_2$, 97%) were used for the synthesis of porous calcium sulphate hemihydrate. Chemical reagents including sodium chloride (NaCl, 99.5%), sodium hydrogen carbonate ($NaHCO_3$, 99.5%), potassium chloride (KCl, 99.5%), dipotassium hydrogen phosphate trihydrate ($K_2HPO_4 \cdot 3H_2O$, 99%), magnesium chloride hexahydrate ($MgCl_2 \cdot 6H_2O$, 98%), sodium sulphate (Na_2SO_4, 99%), tris-hydroxymethyl aminomethane (TRIS, 99%), and hydrochloric acid (HCl) were used for in vitro testing. All reagents were analytical grade and supplied by Sigma Aldrich (St Louis, MO, USA).

Materials for *in vitro* cell studies included Dulbecco's Modified Eagle Medium (DMEM), foetal bovine serum (FBS), penicillin-streptomycin, and Dulbecco's phosphate-buffered saline (DPBS), all purchased from Gibco BRL (Grand Island, NY, USA). The fibroblast cell line (L929) was supplied by ATCC® (USA), and the 3-[4,5-dimethylthiazol-2-yl]-2,5-diphenyl tetrazolium bromide (MTT) kit was obtained from Sigma-Aldrich (St Louis, MO, USA).

2.2. Methods

2.2.1. Preparation of porous-structured alpha-calcium sulphate hemihydrate (α-HH)

Porous α-HH was prepared using a salt solution method. Briefly, $CaCl_2$ solutions with various concentrations (5, 10, 20, and 40% w/v) were prepared by dissolving $CaCl_2$ in deionised water and heating the solution to 110ºC using a magnetic stirrer. Subsequently, the DH precursor (6.5% w/v) was added to the $CaCl_2$ solution at a stirring speed of 250 rpm at 110ºC. The dehydration process of DH to α-HH continued for 90 minutes. The final suspension was then filtered and rinsed several times with boiled distilled water and acetone before being dried at 60ºC for 24 hours. The α-HH samples, derived from different concentrations of $CaCl_2$, were labelled HH5, HH10, HH20, and HH40, respectively.

2.2.2. Characterisation of porous α-HH

Physicochemical characterisation: To examine the physicochemical properties of α-HH, FE-SEM, FTIR, XRD, and TGA/DSC were employed. Crystal morphology and size were imaged using FE-SEM (S4800, Hitachi, Japan) with an acceleration voltage of 10 kV. FTIR spectra were recorded via a spectrometer (Frontier FTIR/NIR, Perkin Elmer Inc., Waltham, MA, USA) within the wavelength range of 4000-400 cm^{-1} to assess structural quality. To investigate phase composition and crystallinity, XRD patterns were obtained using an X-ray diffractometer (D8 Advance Eco, Bruker AXS, Germany) with Cu/Kα radiation (λ = 1.54060 Å) at a scanning rate of 5º/min from 10 to 60º. TGA was conducted in conjunction with DSC to quantify and qualify phase composition in samples within the temperature range of 60-300ºC at a heating rate of 10ºC/min. The percentage of phase consistency was calculated using the following equations (1) and (2) [18]. The three-dimensional structural evaluation was performed by the Archimedes method using water immersion [20, 21].

$$6.2\% \times X + 0\% \times (1 - X) = Y, \text{ when tested sample is comprised of HH and AH} \quad (1)$$

$$6.2\% \times X + 20.9\% \times (1 - X) = Y, \text{ when tested sample is comprised of HH and DH} \quad (2)$$

where X is the percentage of HH in the tested sample (%) and Y is the weight loss percentage (%).

Uniaxial compressive strength characterisation: Uniaxial compressive strength testing was conducted in accordance with ASTM C-472-99 using a universal testing machine. Cylindrical specimens (6 mm in diameter×12 mm in height) were prepared by placing the paste in a mould of appropriate size at 100% relative humidity and 37ºC for setting. Once set, the specimens were removed from the mould and tested using a universal testing machine at a speed of 1 mm/min until failure. Mechanical testing was performed in triplicate (n=3). The uniaxial compressive strength, defined as the maximum compressive stress a material can withstand, was calculated using the equation below:

$$C = \frac{4P}{\pi D^2} \times 10^{-2} \quad (3)$$

where P is the maximum loading force (N), D is the diameter of surface area of sample (cm), and C is the uniaxial compressive strength (MPa).

In vitro degradable and mineralised assessment: The *in vitro* degradation of porous α-HH bioceramic scaffolds was evaluated by immersing the samples in a simulated body fluid (SBF) solution at 37ºC at specific time intervals (0, 1, 3, 5, 7, 14, 21, and 28 days). The SBF solution was formulated to contain ion concentrations closely matching those of human blood plasma, following the protocol in ISO 23317:2014. After each immersion period, the scaffolds were removed from the SBF, washed with deionised water, and dried in a 60ºC oven for weight and pH measurements, as well as morphological characterisation using SEM.

Cytotoxicity by MTT assay: The *in vitro* cytotoxicity of porous α-HH was quantitatively examined using the cytotoxicity test by MTT assay [18]. In short, the test was performed on the extract of the test samples, which was prepared by immersing the test sample in culture media (DMEM) at 37ºC for 72 h. Then, sample extract was filtered through a membrane filter with a pore size of 0.22 µm. After that, the seeded L929 cells at a density of 1×10^4 cells/well were incubated with sample extract, prior to the addition of MTT solution. Then, the solution from the culture plate was discarded before adding 100 µl DMSO to completely dissolve the sediment. Cells incubated with fresh medium (DMEM) or 0.1% SDS were used as a negative control (CN) or positive control (CP), respectively. The absorbance of each well was measured at 570 nm using a microplate reader (HumanReader HS, Human, Germany). The percentage of living cells was calculated according to the following formula:

$$\text{Cell viability (\%)} = \frac{OD_{sample} - OD_{blank}}{OD_{CN} - OD_{blank}} \times 100\% \quad (4)$$

where OD_{sample} and OD_{CN} represent the optical densities of L929 cultured with porous α-HH extract and DMEM, respectively, and OD_{blank} is the optical density of the pure DMEM medium. All measurements were performed in quadruplet.

Cell attachment and migration assay: The attachment and migration of cells on the material were assessed using the Crystal Violet assay [22]. The sample, in powder form, was first placed in a 24-well plate. L929 cells were seeded onto the materials at concentrations of 1500 cells/mg, 3000 cells/mg, and 6000 cells/mg in a culture medium. The culture medium was replaced three times per week until the end of the experiment. Cell adhesion and migration on the material were observed at 4 hours, 3 days, 7 days, and 14 days of incubation. After incubation, samples were fixed with methanol and stained with 0.1% Crystal Violet, then washed twice with DPBS and observed under an inverted microscope (Leica DMi8, Leica Microsystems, Wetzlar, Germany).

3. Results and discussion

3.1. Physicochemical properties of α-HH

The FTIR spectra provided information about the chemical groups in the characterised powder. As shown in Fig. 1A, absorbance peaks at 3610 cm^{-1} and 3550 cm^{-1}, attributed to the vibration of the O-H valence (stretching), were present in the spectra of DH and samples synthesised using various concentrations of $CaCl_2$ solution [23]. These spectra shared the same signature peaks at 1140-1091 cm^{-1} (stretching), 1008 cm^{-1} (stretching), 658 cm^{-1} (bending), and 601 cm^{-1} (bending), which correspond to the vibrations of SO_4^{2-}. In addition, the DH spectra exhibited two strain vibrations at 1684 cm^{-1} and 1620 cm^{-1}, confirming the presence of two types of water molecules in DH [24]. In the spectra of HH5 and HH10, these

two peaks were still detected, indicating the presence of DH in the synthesised powder. Meanwhile, only one bending vibration at 1620 cm^{-1} was displayed in the HH20 and HH40 spectra, demonstrating the successful dehydration of DH into HH. However, it is difficult to conclusively determine whether the obtained HH belonged to the α-form or β-form based solely on the FTIR analysis. Therefore, XRD was suggested for a more definitive conclusion.

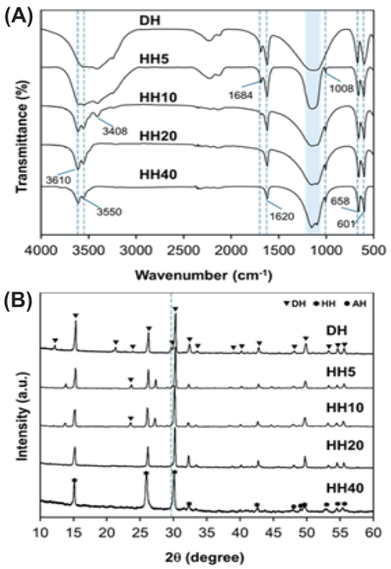

Fig. 1. Structural characterisation of α-HH synthesised over a range of concentrations of $CaCl_2$ solution (w/v) by (A) Fourier transform infrared spectroscopy and (B) X-ray diffraction.

The qualitative XRD analysis of the powders was performed in the range of 2θ=10º to 60º, and the obtained patterns are illustrated in Fig. 1B. As shown in Fig. 1B, the XRD pattern of DH exhibited peaks at 2θ=12.14º, 23.82º, and 29.26º, which are typical peaks of DH as reported in previous studies [18, 25]. The XRD patterns of HH5 and HH10 displayed similar signals to those of DH, while HH20 and HH40 exhibited the dominant sharp peaks of HH, located at 2θ=14.72º, 25.6º, 29.7º, and 32.21º, corresponding to the (200), (020), (400), and (204) lattice planes, respectively [18]. Based on the XRD data, it can be confirmed that $CaCl_2$ concentrations of 20 w/v (HH20) and 40% w/v (HH40) were favourable for the complete conversion of DH into HH, providing evidence that strengthens the earlier conclusions drawn from the FTIR spectra. Furthermore, previous research has indicated that the position of the dominant diffraction peak plays a significant role in determining the crystalline structure of α-HH [26]. In this case, the detected dominant peak of the prepared samples was displayed at 29.7º, which corresponds to the typical peak of α-form, represented by a hexagonal crystal system [26].

The phase analysis of the obtained products was further confirmed by TGA/DSC, which is widely recognised as the most effective method for analysing material processes by assessing mass change through TGA and enthalpy change via DSC. The results are illustrated in Fig. 2, where the black line indicates the TG curve and the red line represents the DSC curve. The TG curve of DH showed a total weight loss of 21.61%, consistent with the theoretical crystal water content in DH (Fig. 2A). The TGA curve of the powder synthesised using 5% $CaCl_2$ (w/v) solution as a crystal growth medium (HH5) showed two transition stages with a total weight loss of 24.54% (Fig. 2B). The first stage, occurring between 100-150ºC, represents the removal of 1.5 water molecules from DH [18]. The TG curve then exhibited a gradual decline in sample weight across a continuous temperature range, corresponding to the removal of 0.5 water molecules [18]. These observations align with two endothermic peaks at 145.83 and 172.36ºC, as indicated in the DSC curve. Meanwhile, a single endothermic peak at 164.64ºC appeared in the DSC curves of HH20 and HH40, demonstrating the successful transformation of the DH crystal phase to the α-HH crystal phase. The theoretical water contents of HH and DH are 6.2 and 20.9%, respectively. HH20 experienced a weight loss of 6.505%, which falls within the range of 6.2-20.9%, indicating 97.93% HH (calculated using Eq. (2)). Similarly, HH40 showed

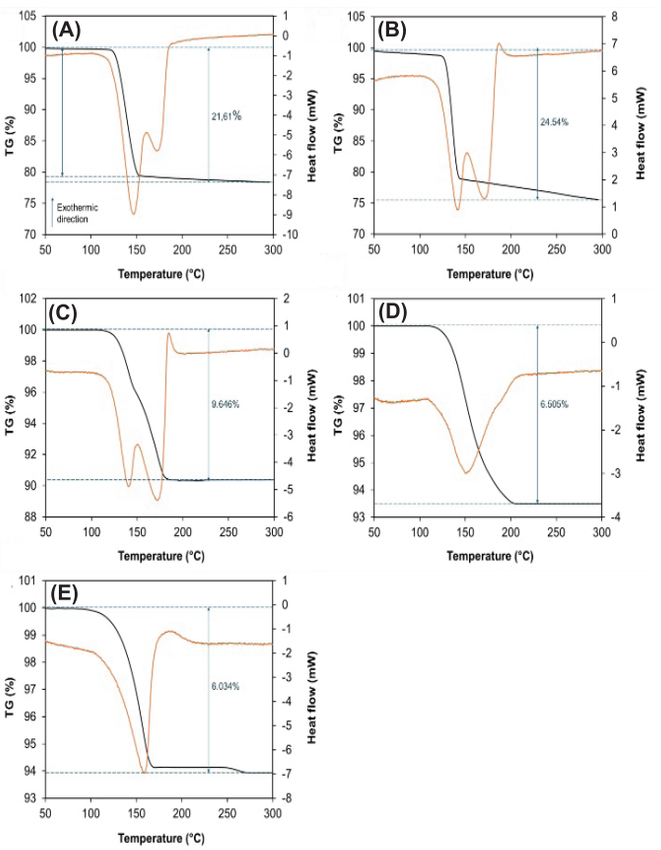

Fig. 2. Phase composition characteristics of α-HH synthesised over a range of concentrations of $CaCl_2$ solution (w/v) thermogravimetric analysis/differential scanning calorimetry: (A) DH, (B) HH5, (C) HH10, (D) HH20, and (E) HH40.

a weight loss of 6.034%, indicating 97.32% HH (calculated using Eq. (1)). These results confirm that α-HH obtained in this study has relatively high purity.

As shown in Fig. 3, the morphology of the synthesised powder was significantly influenced by the $CaCl_2$ concentrations, which ranged from 5-40% (w/v). From Fig. 3, it can be seen that a relatively low concentration of $CaCl_2$ resulted in the incomplete dehydration of DH into HH. In contrast, a supersaturated salt solution was unfavourable for the formation of hexagonal rod-shaped HH crystals with a high aspect ratio. Specifically, as the concentration of $CaCl_2$ solution increased from 5 to 20%, the morphology of the DH precursor gradually transitioned from thick, plate-shaped crystals to hexagonal, rod-shaped crystals in the HH5, HH10, and HH20 samples. This phenomenon can be explained by the accumulation of Ca^{2+} on the end face (001), which led to the elongation of DH wedge crystals, eventually forming hexagonal, rod-shaped crystals [19, 27]. However, when the $CaCl_2$ concentration was increased to 40%, short hexagonal columnar crystals of α-HH, 20-50 µm in length and 5-20 µm in diameter, were observed. This can be attributed to the effect of the solvent on crystalline formation and morphology, which is linked to local supersaturation [14, 28]. In the nucleation stage, higher supersaturation levels generate a greater driving force for nucleus formation, leading to increased nucleation bulk and rates, ultimately resulting in smaller crystal sizes, and *in vitro* testing.

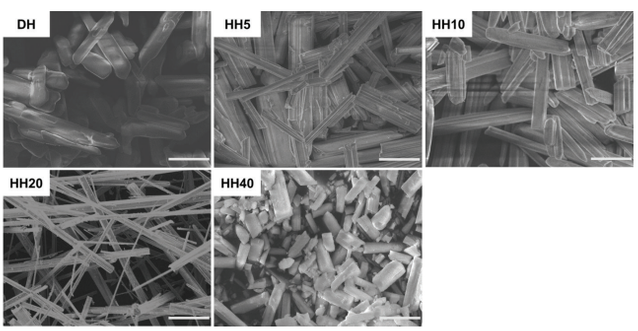

Fig. 3. Scanning electron microscopy images of hemihydrate powders synthesised using various $CaCl_2$ concentrations (w/v). Scale bar: 50 µm.

In summary, the HH20 sample exhibited a rod-shaped crystal structure with a length of 100-250 µm and a diameter of 1-10 µm. The high aspect ratio prevented efficient packing, resulting in voids or spatial interference within the material structure, creating a porous material. The porosity of porous HH20, as measured by Archimedes' principle, was recorded at 61.32%±3.2. The optimal porosity for biological scaffolds used in bone regeneration varies depending on the specific study. While high porosity is beneficial for cell migration and angiogenesis, it can reduce mechanical strength, such as compressive strength, and accelerate scaffold degradation due to the large void volume [29]. Several studies have demonstrated that a porosity range of 60-80% maintains mechanical stability to support physiological loading during the healing process, promoting effective bone regeneration [30, 31]. Therefore, the porosity of the α-HH material in this study is considered to have the potential for effective bone regeneration. Moreover, the α-HH sample exhibited a porous structure with a uniaxial compressive strength of 5.04±0.11 MPa. This value is within the compressive strength range of trabecular bone, making it suitable for non-load-bearing applications. As a result, the HH20 sample was selected for further evaluation of porosity, compressive strength.

3.2. In vitro degradable and biomineralised assessment

Bone remodelling or renewal consists of the resorption of old bone minerals coupled with the formation of new bone simultaneously. In the field of bone regeneration, degradation and biomineralisation are considered fundamental to the success of biodegradable materials. As the scaffold degrades, it should release bioactive ions that promote biomineralisation, aiding the deposition of calcium phosphate apatite on the surface of materials. In both physiological and artificial aqueous environments, bioceramics can degrade via multiple mechanisms: physico-chemical degradation accompanied by a dissolution-reprecipitation phase transformation process, cellular degradation mediated by multinucleated cells (MNCs), and mechanical fragmentation due to a loss of structural integrity resulting from physico-chemical dissolution and cellular degradation [32]. Simulated body fluids (SBF), which mimic human blood plasma, are commonly used as *in vitro* indicators of apatite-forming ability on the surface of materials, predicting the bone-bonding capability of biomaterials. Upon immersion in SBF, interactions occur between the ions released from the samples and those in the SBF. The rapid release of Ca^{2+} ions facilitates an increase in the supersaturation of Ca^{2+} in SBF. These ions tend to combine with phosphate ions (HPO_4^{2-}, PO_4^{3-}) from the SBF to form calcium phosphate apatite. These apatite crystals may also incorporate other ions such as Mg^{2+}, CO_3^{2-}, or organic molecules from SBF, leading to fluctuations in the sample's weight [33]. This process can be summarised by the following equations [34]:

$$9\ CaSO_4.2H_2O + 6\ HPO_4^{2-} \rightarrow Ca_9(PO_4)_5(HPO_4)OH + 6\ H^+ + 9\ SO_4^{2-} + 17\ H_2O \quad (5)$$

or

$$10\ CaSO_4.2H_2O + 6\ HPO_4^{2-} \rightarrow Ca_{10}(PO_4)_6(OH)_2 + 8\ H^+ + 10\ SO_4^{2-} + 18\ H_2O \quad (6)$$

Figure 4A illustrates the time-dependent biodegradability of porous α-HH in SBF at pH 7.4 and 37ºC over 28 days. A rapid increase in weight loss of over 30% was observed within the first 7 days of immersion. After that, the sample's mass slightly increased by 6% during the following 14 days, followed by a significant rise of 11% at the end of the test. This behaviour can be explained by the gradual dissolution of

α-HH, followed and accompanied by the formation of apatite through the precipitation process. The SEM micrographs of the samples at specific time intervals, as depicted in Fig. 4B, strongly confirm this. The images show a porous structure consisting of interlocking crystals in large, irregular particles. The immersion of the samples in SBF resulted in the dissolution of HH, leading to a gradual change in the shape of the crystals from rod-shaped to rough plates over the immersion period. Additionally, the dissolution of α-HH caused a local decrease in pH, which continuously declined from 7.40 to 7.17 during the testing period. This pH reduction promotes demineralisation of the bone surface, exposing growth factors such as BMP and TGF-β, which play key roles in stimulating the formation of new blood vessels and bone regeneration [35]. These findings demonstrate the high potential of this biocompatible bioceramic in bone regeneration applications.

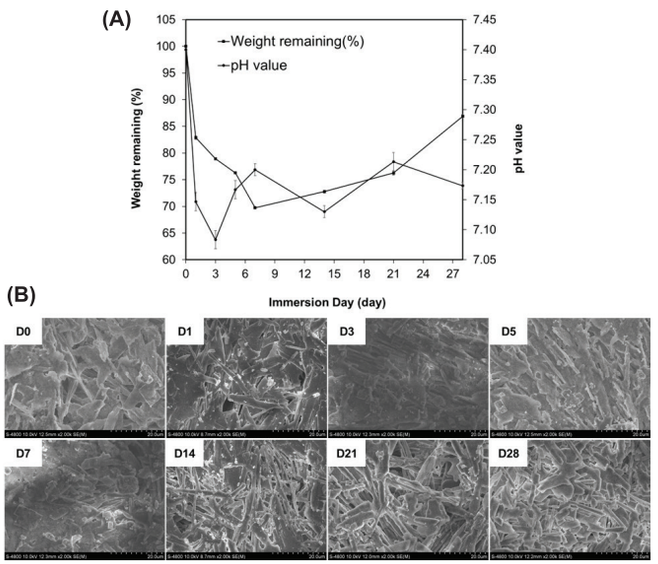

Fig. 4. *In vitro* degradable and biomineralised: (A) degradability of HH20 in simulated body fluid; (B) scanning electron microscopy images of HH20 after being soaked in SBF for 0, 1, 3, 5, 7, 14, 21 and 28 days (n=3).

3.3. Cytotoxicity by 3-[4,5-dimethylthiazol-2-yl]-2,5-diphenyl tetrazolium bromide assay

All biomaterials implanted into the human body must have excellent biocompatibility to prevent immune responses and rejection. Therefore, biocompatibility is a crucial criterion that must be evaluated before practical application. In this study, L929 fibroblasts were chosen as the cell model line to evaluate the in vitro cytocompatibility of HH20, as these cells play essential roles in bone regeneration, including producing and organising the extracellular matrix (ECM) of bone tissue, which provides structural support, promotes new bone growth, and stimulates the proliferation and differentiation of bone-forming cells [36].

The *in vitro* cytotoxicity of porous α-HH was evaluated using MTT, and the results are shown in Fig. 5. L929 fibroblasts were incubated under different conditions, including fresh medium (CN), 1% SDS (CP), HH from a previous study (HH control) [18] and HH20, for comparison. According to the quantitative assays, both HH and HH20 exhibited a relatively high cell survival rate (greater than 90%). This is consistent with previous studies, which report that calcium sulphate-based materials are non-toxic [37, 38]. Furthermore, the cytocompatibility of α-HH was confirmed by morphological observation under an inverted microscope, as shown in Fig. 5B. No significant cell death was observed after treatment with fresh medium, HH, and HH20 at a concentration of 100 mg/ml. Meanwhile, no viable cells were recorded in the CP sample, where most cell morphologies changed from an irregular triangular or spindle shape to a round shape. Based on these observations, it can be concluded that porous α-HH induces no cytotoxic response in L929 fibroblasts and is suitable for medical applications according to ISO 10993-5 (grade 0).

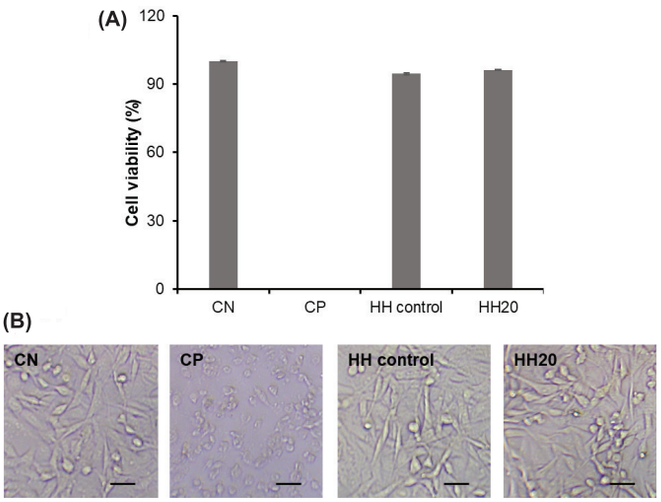

Fig. 5. *In vitro* cytotoxicity analysis of (A) cell viability by 3-[4,5-dimethylthiazol-2-yl]-2,5-diphenyl tetrazolium bromide and (B) cell morphology under an inverted microscope. n=4. Scale bar: 100 μm.

3.4. Cell attachment and migration assay

The ability of cells to adhere to and migrate on the surface of implanted materials is a crucial characteristic for ensuring the material's success. In bone regeneration, cell adhesion to the surface of biomaterials is a significant biological phenomenon that influences various aspects of cell behaviour, including morphology, migration, growth, and differentiation [39]. In this study, cell attachment and migration on porous α-HH were assayed using the L929 cell line at three different densities for 4 hours, 3 days, 7 days, and 14 days, using the Crystal Violet staining method, followed by observation under an inverted microscope (Fig. 6).

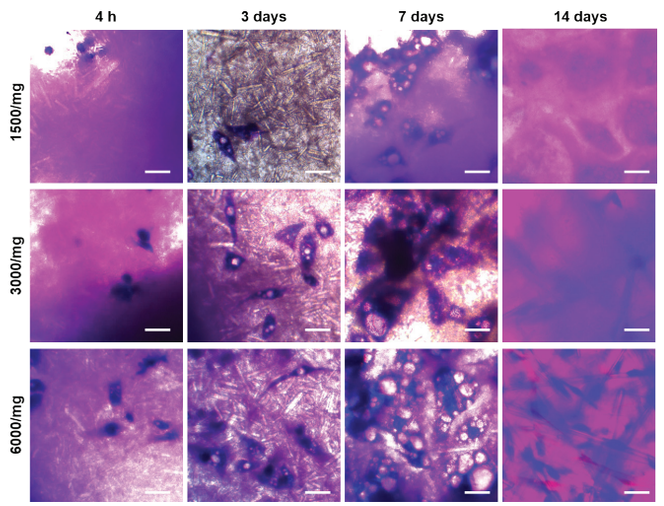

Fig. 6. Cell adhesion ability of HH20 materials by crystal violet staining. Scale bar: 100 µm.

The Crystal Violet qualitative assessment of fibroblasts showed that after 4 hours of seeding, the cell shape appeared similar across all cell densities and resembled the typical morphology of L929 fibroblasts. Over time, the number of cells increased, with some already spreading across the surface of the materials by the third day of culture. Notably, the characteristic shape of the L929 fibroblasts was not observed as the cultivation period was prolonged. At 7 and 14 days post-seeding, higher cellular viability was observed on the material surface, with cells adopting a flattened shape. These cells tended to cluster, forming tissue-like aggregates, illustrated by the large, dark purple areas. The extent and intensity of these purple regions were more pronounced at 14 days than at 7 days post-seeding, demonstrating the material's long-term effectiveness in promoting cell adhesion, migration, and proliferation. This may be attributed to the partial degradation of the porous α-HH, creating additional voids and increasing the proportion of free space for cell penetration. The results of this study indicate that the porous α-HH manufactured using the proposed process enhances cell adhesion, migration, and growth, which are essential for promoting bone regeneration.

4. Conclusions

In this study, to enhance the porosity and quality of bone regeneration materials, the salt solution method using only high concentrations of $CaCl_2$ was applied to synthesise high-aspect-ratio α-HH crystals. $CaCl_2$ solutions were investigated at various concentrations, including 5, 10, 20, and 40%. The results of FTIR, XRD, TGA/DSC, and SEM analyses showed that at a 20% concentration, the α-HH material (HH20) exhibited the compositional characteristics of α-HH and achieved a high-aspect-ratio hexagonal rod-like crystal structure, resulting in structural porosity with a value of 61.32%±3.2 and a uniaxial compressive strength of 5.04±0.11 MPa. Moreover, the porous-structured α-HH was proven to be medical grade and demonstrated rapid degradation along with a favourable pH alteration profile, stimulating both biological and chemical transformations of cells during the bone formation process. Furthermore, *in vitro* cell studies using L929 fibroblastic cell lines demonstrated migration, with cells adhering to the porous α-HH bioceramic. This indicates that the distribution and morphology of α-HH crystals can be controlled to enhance the porous structure of α-HH ceramics, improving cell adhesion and migration for bone regeneration applications. These findings suggest that the salt solution method using a high concentration of $CaCl_2$ is a suitable approach for synthesising α-HH materials with optimal porous properties, offering great potential for use in bone regeneration applications.

CRediT author statement

Anh Phuong Nguyen Hong: Formal analysis, Methodology, Software, Conceiving and designing the analysis, Visualisation, Writing - Original draft preparation; Dieu Linh Tran: Methodology, Conceiving and designing the analysis, Data curation, Software; Ngoc Thuy Trang Le: Visualisation, Performing the analysis; Quoc Vinh Ho: Formal analysis, Software; Minh Hoang Vo Do: Conceiving and designing the analysis; Dang Khoa Vo Nguyen: Contributing data or analysis tools; Van Du Cao: Methodology, Conceiving and designing the analysis; Dai Hai Nguyen: Investigation, Funding acquisition, Supervision, Writing, Reviewing, Editing.

ACKNOWLEDGEMENTS

This research was supported by Ministry of Science and Technology, Vietnam under Grant No. DTDL.CN-35/22.

COMPETING INTERESTS

The authors declare that there is no conflict of interest regarding the publication of this article.

REFERENCES

[1] I. Roohani, G.C. Yeo, S.M. Mithieux, et al. (2022), "Emerging concepts in bone repair and the premise of soft materials", *Current Opinion in Biotechnology*, **74**, pp.220-229, DOI: 10.1016/j.copbio.2021.12.004.

[2] M. Bahraminasab (2020), "Challenges on optimization of 3D-printed bone scaffolds", *BioMedical Engineering Online*, **19(1)**, DOI: 10.1186/s12938-020-00810-2.

[3] J.L. Hernandez, K.A. Woodrow (2022), "Medical applications of porous biomaterials: Features of porosity and tissue-specific implications for biocompatibility", *Advanced Healthcare Materials*, **11(9)**, DOI: 10.1002/adhm.202102087.

[4] M. Ebrahimi (2021), "Porosity parameters in biomaterial science: Definition, impact, and challenges in tissue engineering", *Frontiers of Materials Science*, **15(3)**, pp.352-373, DOI: 10.1007/s11706-021-0558-4.

[5] Z. Miri, H.J. Haugen, D. Loca, et al. (2024), "Review on the strategies to improve the mechanical strength of highly porous bone bioceramic scaffolds", *Journal of The European Ceramic Society*, **44(1)**, pp.23-42, DOI: 10.1016/j.jeurceramsoc.2023.09.003.

[6] H. Mohammadi, M. Sepantafar, N. Muhamad, et al. (2021), "How does scaffold porosity conduct bone tissue regeneration?", *Advanced Engineering Materials*, **23(10)**, DOI: 10.1002/adem.202100463.

[7] I. Berbezier, M.D. Crescenzi (2015), "Self-assembly of nanostructures and nanomaterials", *Beilstein Journal of Nanotechnology*, **6**, pp.1397-1398, DOI: 10.3762/bjnano.6.144.

[8] S. Chang, X. Wang, Q. Hu, et al. (2022), "Self-assembled nanocomposites and nanostructures for environmental and energy applications", *Crystals*, **12(2)**, DOI: 10.3390/cryst12020274.

[9] A.D. Escudero, M. Espanol, M.P. Ginebra (2024), "High-aspect-ratio nanostructured hydroxyapatite: Towards new functionalities for a classical material", *Chemical Science*, **15(1)**, pp.55-76, DOI: 10.1039/D3SC05344J.

[10] R. Ene, M. Nica, D. Ene, et al. (2021), "Review of calcium-sulphate-based ceramics and synthetic bone substitutes used for antibiotic delivery in PJI and osteomyelitis treatment", *EFORT Open Reviews*, **6(5)**, pp.297-304, DOI: 10.1302/2058-5241.6.200083.

[11] A. Ślósarczyk, J. Czechowska, Z. Paszkiewicz, et al. (2010), "New bone implant material with calcium sulphate and Ti modified hydroxyapatite", *Journal of Achievements in Materials and Manufacturing Engineering*, **43(1)**, pp.170-177.

[12] N. Eliaz, N. Metoki (2017), "Calcium phosphate bioceramics: A review of their history, structure, properties, coating technologies and biomedical applications", *Materials*, **10(4)**, DOI: 10.3390/ma10040334.

[13] D. Yang, Y. Yan, X. Liu, et al. (2018), "Characterization of an α-calcium sulphate hemihydrates/α-tricalcium phosphate combined injectable bone cement", *ACS Applied Bio Materials*, **1(3)**, pp.768-776, DOI: 10.1021/acsabm.8b00221.

[14] Z. Pan, Y. Lou, G. Yang, et al. (2013), "Preparation of calcium sulphate dihydrate and calcium sulphate hemihydrate with controllable crystal morphology by using ethanol additive", *Ceramics International*, **39(5)**, pp.5495-5502, DOI: 10.1016/j.ceramint.2012.12.061.

[15] M. Tang, X. Shen, H. Huang (2010), "Influence of α-calcium sulphate hemihydrate particle characteristics on the performance of calcium sulphate-based medical materials", *Materials Science and Engineering: C*, **30(8)**, pp.1107-1111, DOI: 10.1016/j.msec.2010.06.006.

[16] C. Hazra, S. Bari, D. Kundu, et al. (2014), "Ultrasound-assisted/biosurfactant-templated size-tunable synthesis of nano-calcium sulphate with controllable crystal morphology", *Ultrasonics Sonochemistry*, **21(3)**, pp.1117-1131, DOI: 10.1016/j.ultsonch.2013.12.020.

[17] G. Jiang, Q. Chen, C. Jia, et al. (2015), "Controlled synthesis of monodisperse α-calcium sulphate hemihydrate nanoellipsoids with a porous structure", *Physical Chemistry Chemical Physics*, **17(17)**, pp.11509-11515, DOI: 10.1039/C5CP00804B.

[18] D.L. Tran, A.P.N. Hong, N.H. Nguyen, et al. (2023), "α-calcium sulphate hemihydrate bioceramic prepared via salt solution method to enhance bone regenerative efficiency", *Journal of Industrial and Engineering Chemistry*, **120**, pp.293-301, DOI: 10.1016/j.jiec.2022.12.036.

[19] M.M. Mbogoro, M. Peruffo, M.A. Vidal, et al. (2017), "Quantitative 3D visualization of the growth of individual gypsum microcrystals: Effect of Ca_2^+:SO_4^{2-} ratio on kinetics and crystal morphology", *The Journal of Physical Chemistry C*, **121(23)**, pp.12726-12734, DOI: 10.1021/acs.jpcc.7b01566.

[20] H.Y. Yeung, L. Qin, K.M. Lee, et al. (2007), "Quantification of porosity, connectivity and material density of calcium phosphate ceramic implants using micro-computed tomography", *Advanced Bioimaging Technologies in Assessment of The Quality of Bone and Scaffold Materials*, pp.289-305, DOI: 10.1007/978-3-540-45456-4_17.

[21] A. Arifin, Gunawan, A. Priyadi, et al. (2020), "Development and characterization of porous hydroxyapatite-Alumina composite for engineering application", *IOP Conference Series: Materials Science and Engineering*, **857(1)**, DOI: 10.1088/1757-899X/857/1/012005.

[22] D. Bellucci, E. Veronesi, V. Strusi, et al. (2019), "Human mesenchymal stem cell combined with a new strontium-enriched bioactive glass: An *ex-vivo* model for bone regeneration", *Materials*, **12(21)**, DOI: 10.3390/ma12213633.

[23] N.T.N. Le, N.T.T. Le, Q.L. Nguyen, et al. (2020), "A facile synthesis process and evaluations of α-calcium sulphate hemihydrate for bone substitute", *Materials*, **13(14)**, DOI: 10.3390/ma13143099.

[24] P.K. Mandal, T.K. Mandal (2002), "Anion water in gypsum ($CaSO_4 \cdot 2H_2O$) and hemihydrate ($CaSO_4 \cdot 1/2H_2O$)", *Cement and Concrete Research*, **32(2)**, pp.313-316, DOI: 10.1016/S0008-8846(01)00675-5.

[25] Y. Wang, X. Mao, C. Chen, et al. (2020), "Effect of sulfuric acid concentration on morphology of calcium sulphate hemihydrate crystals", *Materials Research Express*, **7(10)**, DOI: 10.1088/2053-1591/abbc41.

[26] X. Zhang, L. Ran, X. Wang, et al. (2022), "Structural characteristic and formation mechanism of hemihydrate calcium sulphate whiskers prepared using FGD gypsum", *Particuology*, **62**, pp.98-103, DOI: 10.1016/j.partic.2021.04.010.

[27] P. Wang, E. Lee, C. Park, et al. (2008), "Calcium sulphate hemihydrate powders with a controlled morphology for use as bone cement", *Journal of The American Ceramic Society*, **91(6)**, pp.2039-2042, DOI: 10.1111/j.1551-2916.2008.02358.x.

[28] B. Guan, G. Jiang, Z. Wu, et al. (2011), "Preparation of α-calcium sulphate hemihydrate from calcium sulphate dihydrate in methanol-water solution under mild conditions", *Journal of The American Ceramic Society*, **94(10)**, pp.3261-3266, DOI: 10.1111/j.1551-2916.2011.04470.x.

[29] J. Zhou, S. Xiong, M. Liu, et al. (2023), "Study on the influence of scaffold morphology and structure on osteogenic performance", *Frontiers in Bioengineering and Biotechnology*, **11**, DOI: 10.3389/fbioe.2023.1127162.

[30] J. Jiao, Q. Hong, D. Zhang, et al. (2023), "Influence of porosity on osteogenesis, bone growth and osteointegration in trabecular tantalum scaffolds fabricated by additive manufacturing", *Frontiers in Bioengineering and Biotechnology*, **11**, DOI: 10.3389/fbioe.2023.1117954.

[31] Y. Zhang, N. Sun, M. Zhu, et al. (2022), "The contribution of pore size and porosity of 3D printed porous titanium scaffolds to osteogenesis", *Biomaterials Advances*, **133**, DOI: 10.1016/j.msec.2022.112651.

[32] N.L. Davison, F.B.D. Groot, D.W. Grijpma (2014), "Degradation of biomaterials", *Tissue Engineering,* Second Edition, pp.177-215, DOI: 10.1016/B978-0-12-420145-3.00006-7.

[33] N. Strutynska, O. Livitska, S. Prylutska, et al. (2020), "New nanostructured apatite-type (Na^+, Zn^{2+}, CO_3^{2-}) - doped calcium phosphates: Preparation, mechanical properties and antibacterial activity", *Journal of Molecular Structure*, **1222**, DOI: 10.1016/j.molstruc.2020.128932.

[34] M. Bohner (2004), "New hydraulic cements based on α-tricalcium phosphate-calcium sulphate dihydrate mixtures", *Biomaterials*, **25(4)**, pp.741-749, DOI: 10.1016/S0142-9612(03)00573-8.

[35] L. Panahipour, A. Omerbasic, J. Nasirzade, et al. (2021), "TGF-β activity of a demineralized bone matrix", *International Journal of Molecular Sciences*, **22(2)**, DOI: 10.3390/ijms22020664.

[36] H. Wang, L. Qi, C. Shema, et al. (2024), "Advances in the role and mechanism of fibroblasts in fracture healing", *Frontiers in Endocrinology*, **15**, DOI: 10.3389/fendo.2024.1350958.

[37] H. Hsu, R.A. Waris, M. Ruslin, et al. (2018), "An innovative α-calcium sulphate hemihydrate bioceramic as a potential bone graft substitute", *Journal of The American Ceramic Society*, **101(1)**, pp.419-427, DOI: 10.1111/jace.15181.

[38] Y. Lou, F. Cheng, Y. Zhang (2020), "Preparation and characterization of α-calcium sulphate hemihydrate (CSH)/marine shells scaffold with cervus and cucumis polypeptide composite biomaterials for bone reconstruction", *Journal of Biomaterials and Tissue Engineering*, **10(1)**, pp.17-25, DOI: 10.1166/jbt.2020.2253.

[39] H.I. Chang, Y. Wang (2011), "Cell responses to surface and architecture of tissue engineering scaffolds", *Regenerative Medicine and Tissue Engineering - Cells and Biomaterials*, DOI: 10.5772/21983.